Atmos. Chem. Phys., 25, 1273–1287, 2025
https://doi.org/10.5194/acp-25-1273-2025
© Author(s) 2025. This work is distributed under
the Creative Commons Attribution 4.0 License.

Atmospheric Chemistry and Physics
Open Access
EGU

Research article

Quasi-weekly oscillation of regional $PM_{2.5}$ transport over China driven by the synoptic-scale disturbance of the East Asian winter monsoon circulation

Yongqing Bai[1], Tianliang Zhao[2], Kai Meng[3], Yue Zhou[1], Jie Xiong[1], Xiaoyun Sun[4], Lijuan Shen[5], Yanyu Yue[1], Yan Zhu[1], Weiyang Hu[6], and Jingyan Yao[2]

[1]China Meteorological Administration Basin Heavy Rainfall Key Laboratory, Hubei Key Laboratory for Heavy Rain Monitoring and Warning Research, Institute of Heavy Rain, China Meteorological Administration, Wuhan 430205, China
[2]Climate and Weather Disasters Collaborative Innovation Center, Key Laboratory for Aerosol-Cloud-Precipitation of China Meteorological Administration, Nanjing University of Information Science & Technology, Nanjing 210044, China
[3]Key Laboratory of Meteorology and Ecological Environment of Hebei Province, Hebei Provincial Institute of Meteorological Sciences, Shijiazhuang 050021, China
[4]Anhui Province Key Laboratory of Atmospheric Science and Satellite Remote Sensing, Anhui Institute of Meteorological Sciences, Hefei 230031, China
[5]School of Atmosphere and Remote Sensing, Wuxi University, Wuxi 214105, China
[6]State Key Laboratory of Pollution Control and Resource Reuse and School of the Environment, Nanjing University, Nanjing 210023, China

Correspondence: Tianliang Zhao (tlzhao@nuist.edu.cn) and Kai Meng (macka@foxmail.com)

Received: 7 August 2024 – Discussion started: 18 September 2024
Revised: 10 November 2024 – Accepted: 5 December 2024 – Published: 29 January 2025

Abstract. Regional $PM_{2.5}$ transport is an important cause of atmospheric environment change. However, the variations in regional $PM_{2.5}$ transport on a synoptic scale with meteorological drivers have been incomprehensively understood. Therefore, this study is targeted at the quasi-weekly oscillation (QWO) of regional $PM_{2.5}$ transport over central and eastern China (CEC) with the influence of synoptic-scale disturbance of the East Asian winter monsoon (EAWM) circulation. By constructing the data of daily $PM_{2.5}$ transport flux in CEC in the winters of 2015–2019, we utilize the extended empirical orthogonal function (EEOF) decomposition and other statistical methods to extract the moving spatial distribution of regional $PM_{2.5}$ transport over CEC, recognizing the QWO in regional $PM_{2.5}$ transport with the spatial–temporal variations over CEC. The source–receptor relationship in regional transport of $PM_{2.5}$ is identified with the 2 d lag effect of the North China Plain, as the upwind source region, on the $PM_{2.5}$ pollution change in the Twain-Hu Basin, as the downwind receptor region in central China. The QWO of regional $PM_{2.5}$ transport over CEC is regulated by the synoptic-scale disturbance of the EAWM circulation with the periodic activities of the Siberian high. These findings provide new insights into the understanding of regional $PM_{2.5}$ transport with the source–receptor relationship and the meteorological mechanism in atmospheric environment change.

Published by Copernicus Publications on behalf of the European Geosciences Union.

1 Introduction

$PM_{2.5}$ pollution has attracted worldwide attention due to its adverse impact on the environment and human health (Fan et al., 2016; Geng et al., 2021; Lin et al., 2018). $PM_{2.5}$ pollution in the cold season has become a major atmospheric environmental problem in China (An et al., 2019; Huang et al., 2020b). High-concentration $PM_{2.5}$ tends to occur with extensive spatiotemporal coverage (Tao et al., 2016; Zhang et al., 2019), and synthetic physical–chemical processes cause such heavy $PM_{2.5}$ pollution events (Ding et al., 2017; Quan et al., 2020), including emissions (Liu et al., 2016; Zheng et al., 2018a), chemical formation (Huang et al., 2014; Nie et al., 2014), atmospheric boundary layer processes (Huang et al., 2018; Zhong et al., 2018), and localized circulation (Miao et al., 2015; Shu et al., 2021; Zheng et al., 2018b), as well as weather and climate (Cai et al., 2017; Wu et al., 2016). The interactions among these physical and chemical processes make it more challenging to comprehend severe haze formation, which serves as one of the major difficulties in forecasting and controlling atmospheric environment change and heavy air pollution (Zhang et al., 2012; Zhang et al., 2019).

$PM_{2.5}$ has with complex spatiotemporal changes on multiple scales (Georgoulias and Kourtidis, 2012; Wu et al., 2021). $PM_{2.5}$ oscillates periodically at multiple timescales, and the periodic oscillation of atmospheric circulation is the leading cause of the cyclical variations in $PM_{2.5}$ (Chen et al., 2020; Dong et al., 2021; Fu et al., 2020; Perrone et al., 2018). To be specific, the 1 d periodic change or diurnal variation in near-surface $PM_{2.5}$ concentrations is mainly attributed to atmospheric boundary layer processes and localized circulation (Miao et al., 2019); the periodic change of around 7 d may be controlled by the fluctuation of the longwave trough in middle and high latitudes (Guo et al., 2014); the oscillating cycle of about 14 d is closely related to the quasi-biweekly oscillation of the synoptic circulation (Gao et al., 2020; Zhao et al., 2019); and the 30–60 d intra-seasonal oscillation is mainly caused by the impact of monsoon circulation change (Xu et al., 2014; Zhang et al., 2019). Comprehensively revealing the interaction between $PM_{2.5}$ and meteorology at different timescales is essential for solving air pollution problems more effectively (Bäumer and Vogel, 2007; Wang et al., 2020). Previous studies, which mainly focused on the multiscale periodic variation in atmospheric pollutants in a certain region or local area, have not yet investigated the $PM_{2.5}$ trans-regional and periodic oscillation in the large area of central and eastern China (CEC).

The East Asian winter monsoon (EAWM) is one of the most active atmospheric circulation systems in the cold season over the Northern Hemisphere (Ding et al., 2017; Wu and Wang, 2002), which is also a critical leading factor for the variation in wintertime air pollution in CEC (Chin, 2012; Li et al., 2016). Being a major circulation system of the EAWM, the Siberian high dominates the cold seasons, acting as a particular driver of cold airflows, thus having an important impact on the wintertime atmospheric environment in CEC (An et al., 2019; Shen et al., 2021, 2022; Wu et al., 2016). The rapid southward advance of cold air with the strong Siberian high can effectively drive the regional transport of air pollutants with less accumulation across CEC, while the weak Siberian high with the slow southward movement of cold air can be particularly favorable for the transport of air pollutants from the northern source regions to southern receptor region over CEC (Hou et al., 2020; Zhang et al., 2016). When the position of the Siberian high is more eastern than normal, the transport of air pollutants from northern China to the south is weakened, and the aggravation of pollution is enhanced in northern China (Jia et al., 2015). Regional pollutant transport driven by the southward movement of a cold front with the Siberian high would exacerbate the air quality in the corresponding receptor regions (Kang et al., 2019; Hu et al., 2021; Shen et al., 2022). The characteristics of atmospheric circulation anomalies favoring heavy haze pollution in China have changed in recent years, and the leading formation mechanism of severe haze has been shifting from local accumulation to regional transport processes in eastern China (Yang et al., 2021b). Therefore, studying the influence of the EAWM circulation system on regional pollutant transport over CEC is an important issue in atmospheric environment changes (Bai et al., 2021, 2022; Ge et al., 2018; Merrill and Kim, 2004; Tan et al., 2021; Yang, et al., 2021a).

Previous studies have primarily focused on the relationship between atmospheric intraseasonal oscillations in the mid-latitudes to high latitudes of the Eurasian region and persistent $PM_{2.5}$ pollution (An et al., 2022; Gao et al., 2020; Li et al., 2021; Liu et al., 2022; Wu et al., 2023; Yang et al., 2024b). $PM_{2.5}$ concentration anomalies in north China exhibit significant lifetimes of 10–30 d, with anticyclonic anomalies and related meteorological conditions (e.g., surface air temperature, boundary layer height) in northeast Asia influencing local $PM_{2.5}$ accumulation and hygroscopic growth (An et al., 2022; Yang et al., 2024b). These studies have investigated the quasi-biweekly life cycle of persistent $PM_{2.5}$ pollution events in north China through phase synthesis methods (Gao et al., 2020; Wu et al., 2023; Yang et al., 2024b). However, there remains a lack of systematic studies on the synoptic-scale oscillation of regional $PM_{2.5}$ transport.

The "harbor" effect on the eastern lee of the Tibetan Plateau's large topography on the westerlies is possibly an important factor influencing the regional distribution of $PM_{2.5}$ pollution in CEC with weak horizontal winds and sinking motion in the lower troposphere, which exacerbates the environmental impacts of local air pollutant emissions, establishing a "susceptibility zone" in this region (Xu et al., 2016; Zhu et al., 2018). Anticyclones and cyclones alternatively affect the region on a timescale of 3–7 d, resulting in periodic air pollution in cities (Guo et al., 2014). Thus, the weather system in CEC is basically characterized by periodic changes and cold air in winter, with the EAWM oscillating in

quasi-weekly periods (Wu and Wang, 2002; Wu et al., 2016). However, the influence of the synoptic-scale disturbance of the EAWM on regional $PM_{2.5}$ transport over CEC is not yet clear. Responding to this problem, this study aims to reveal from a new perspective the quasi-weekly oscillation (QWO) of regional $PM_{2.5}$ transport over CEC affected by the EAWM and its underlying mechanism with the synoptic-scale oscillation of the EAWM circulation. This study could deepen the understanding of regional $PM_{2.5}$ transport, its source–receptor relationship, and its meteorological mechanism in the atmospheric environment changes and provide scientific evidence for air pollution forecast, early warning, and coordinated control.

2 Data and methods

2.1 Environmental and meteorological data

The daily dataset of $PM_{2.5}$ concentrations selected for this study was from the China National Environmental Monitoring Center (https://quotsoft.net/air/, last access: 27 January 2025), including daily $PM_{2.5}$ concentrations from 1079 air quality monitoring stations in CEC during the winters (December–February) of 2015–2019.

Meteorological data were selected from the NCEP/NCAR global reanalysis daily data (https://psl.noaa.gov/data/gridded/tables/daily.html, last access: 27 January 2025) with a grid resolution of $2.5° \times 2.5°$ for the large-scale circulation analysis. It is composed of the daily sea level pressure (SLP), air temperature at 1000 hPa, and the U and V components of wind at 1000 hPa during the winters of 2015–2019.

In addition, the ERA5-Land high-resolution reanalysis hourly dataset (https://cds.climate.copernicus.eu/cdsapp#!/dataset/reanalysis-era5-land?tab=form, last access: 27 January 2025) with a spatial resolution of $0.1° \times 0.1°$ was selected for the calculation of transport flux (TF) of $PM_{2.5}$ in CEC. The U and V components of the 10 m wind over CEC were obtained at 00:00, 06:00, 12:00, and 18:00 UTC daily during the winter (December–February) of 2015–2019. In order to match the resolution of $PM_{2.5}$ daily data, the ERA5-Land high-resolution 10 m wind was processed into daily average data.

2.2 $PM_{2.5}$ TF and its divergence

In order to quantitatively characterize the horizontal transport direction and intensity of $PM_{2.5}$ as well as convergence or divergence during regional $PM_{2.5}$ transport, we introduced the concepts of $PM_{2.5}$ TF and divergence of $PM_{2.5}$ TF. Generally, there are two types of TF: horizontal and vertical. This study only addresses the near-surface horizontal $PM_{2.5}$ TF. The horizontal $PM_{2.5}$ TF is defined as the $PM_{2.5}$ mass passing through the unit area in unit time (unit: $\mu g\,m^{-2}\,s^{-1}$), expressed as the product of wind vector and $PM_{2.5}$ concentration (Liu et al., 2019; Ma et al., 2021), and its vector points to the same direction as the horizontal wind. The zonal component (F_u) and meridional component (F_v) of the $PM_{2.5}$ TF vector (TFV) and the TF magnitude (TFM) are calculated as follows:

$$F_u = C \cdot u \tag{1}$$

$$F_v = C \cdot v \tag{2}$$

$$\mathrm{TFV} = F_u\, i + F_v\, j \tag{3}$$

$$\mathrm{TFM} = \sqrt{F_u^2 + F_v^2}, \tag{4}$$

where C is the surface $PM_{2.5}$ concentration, and u and v are the zonal and meridional components of the 10 m wind speed, respectively.

Firstly, the U and V components of ERA5-Land high-resolution 10 m wind are interpolated to 1079 stations of environmental measurements in CEC for calculations of near-surface $PM_{2.5}$ TF in this study. Then, the daily $PM_{2.5}$ TF of the 1079 stations for the winters from 2015 to 2019 is calculated according to the calculation by Formulas (1)–(4).

The divergence of $PM_{2.5}$ TF can be an indicator for the $PM_{2.5}$ budget. When positive divergence occurs, the air pollutants were net outflow from the domain region, and vice versa (Wang et al., 2021). The divergence of horizontal $PM_{2.5}$ TF near the surface is calculated as follows (Wang et al., 2021):

$$D = \frac{\partial F_u}{\partial x} + \frac{\partial F_v}{\partial y}, \tag{5}$$

where D is the horizontal $PM_{2.5}$ TF divergence (unit: $\mu g\,m^{-3}\,s^{-1}$). If D is positive (negative), it indicates divergence (convergence) of $PM_{2.5}$ TF.

In the i and j grids, the expression of Formula (5) for the differential calculation with d the grid spacing is

$$D = \frac{Fu_{i+1,j} - Fu_{i-1,j} + Fv_{i,j+1} - Fv_{i,j-1}}{2d}. \tag{6}$$

When calculating the horizontal divergence of the transport $PM_{2.5}$ flux, it is necessary to interpolate the station data of zonal and meridional components (F_u, F_v) of $PM_{2.5}$ TFV to grid spacing with 0.25 by 0.25° in longitude and latitude in CEC and then calculate the divergence of $PM_{2.5}$ TF at each grid point according to Formula (6).

2.3 Butterworth filter

Atmospheric motion encompasses a variety of temporal and spatial scales. The sequences of meteorological variables often contain complex periodic components and exhibit multiple-timescale variations, including daily, weekly, seasonal, and interannual variations. Numerous observations have found the QWO with periods of less than 10 d across various meteorological elements in the EAWM system (Compo et al., 1999; Murakami, 1979; Wu and Wang,

2002). Synoptic-scale atmospheric variations are closely related to atmospheric longwave adjustments, with QWO periods of 4–7 d observed in cold-air activities of the EAWM (Bai et al., 2022; Wu and Wang, 2002). The synoptic-scale disturbance regulates the generation, transport, and removal of $PM_{2.5}$ in air pollution, which is a key mechanism behind the 4–7 d periodic changes in $PM_{2.5}$ in CEC during the periods of the EAWM (Guo et al., 2014; Liu et al., 2018; Quan et al., 2014, 2020). Based on the research objectives, identifying the desired periodic components from the original observational sequences is referred to as sequence filtering. In this study, we employed a Butterworth filter to extract the QWO from observational data.

The Butterworth filter is commonly used to separate atmospheric periodic variations across specific frequency bands. Due to its smooth amplitude response, linear phase characteristics, and ease of implementation, the Butterworth filter has been widely applied in climate and meteorological studies (Gouirand et al., 2012; Yang et al., 2024a). The Butterworth filter can be configured as a low-pass, high-pass, or band-pass filter, depending on the specific requirements. A band-pass filter only allows signals within a defined frequency range to pass through with attenuating signals outside the defined frequency range. It is often employed to extract and analyze signals within specific frequency bands, such as particular weather patterns and climate cycles. In this study, to investigate the QWO (8 d) of regional $PM_{2.5}$ transport over CEC under the influence of the EAWM circulation on the synoptic scale, we applied Butterworth band-pass filtering to the daily TFM of $PM_{2.5}$ change and daily SLP anomalies during the winters of 2015–2019 for identifying the quasi-weekly (6–9 d) synoptic-scale component of regional transport of $PM_{2.5}$ over CEC.

2.4 Extended empirical orthogonal function (EEOF)

The empirical orthogonal function (EOF) analysis is a widely applied climate statistical method in atmospheric and oceanographic scientific studies (Kim and Ha, 2015; Li et al., 2019; Schepanski et al., 2016), also used to investigate the variability of atmospheric aerosols at different spatiotemporal scales (Bai et al., 2022; Feng et al., 2020). The mathematical process of EOF analysis is to decompose the variable field $X_{m\times n}$, which consists of observations at n times at m spatial points, into a linear combination of p spatial eigenvectors (modes) with corresponding time-weighting coefficients:

$$X_{m\times n} = V_{m\times p} T_{p\times n}, \tag{7}$$

where V is the spatial eigenvector (load), and T represents the time coefficient. The main information of the variable field $X_{m\times n}$ is represented by several eigenvectors. Since the method has been widely applied, the detailed calculation steps of EOF decomposition are omitted here, and our focus is on how to construct the observation matrix.

Firstly, we decompose the daily $PM_{2.5}$ TFM anomalies of 1079 stations in CEC during the winters of 2015–2019 using the EOF method. Thus, the following observation matrix can be obtained:

$$X = \begin{bmatrix} x_{11}\cdots x_{1n} \\ \vdots \\ x_{m1}\cdots x_{mn} \end{bmatrix}, \tag{8}$$

where X represents the $PM_{2.5}$ TFM anomalies, m represents the spatial points for 1079 stations, and n represents the observation times of 450 d. Then, the variable field X is decomposed into the sum of the product of space and time functions according to Formula (7).

EOF decomposition of $PM_{2.5}$ TFV anomalies can be performed by employing the complex matrix; hence the following observation matrix is constructed:

$$X = \begin{bmatrix} u_{11}\cdots u_{1n} \\ \vdots \\ u_{m1}\cdots u_{mn} \\ v_{11}\cdots v_{1n} \\ \vdots \\ v_{m1}\cdots v_{mn} \end{bmatrix}, \tag{9}$$

where X is the $PM_{2.5}$ TFV anomalies, and u and v refer to the zonal and meridional components of TFV anomalies.

With EOF analysis we can get the spatial distribution structure, which is in a fixed time pattern of climate variables, but we cannot get a temporally moving spatial distribution structure. The EEOF is an extension of the EOF to analyze the autocorrelations of the variable field over time. By selecting a lag time, the original observational matrix is expanded into multiple continuous time matrices, diagnosing the temporal changes in the spatial structure of variable fields. This method has widespread applications in the analysis and prediction of marine and atmospheric motions (Dey et al., 2018; Qian et al., 2019; Wang et al., 2019).

In this study, we utilized the EEOF analysis to reveal the evolution of $PM_{2.5}$ TF to reveal the spatiotemporal variations in regional $PM_{2.5}$ transport. On the basis of Formula (8), a new extension matrix of the $PM_{2.5}$ TFM is constructed. Due to the study on the synoptic scale, five lag times are selected, and each lag time is 1 d in length. The constructed observa-

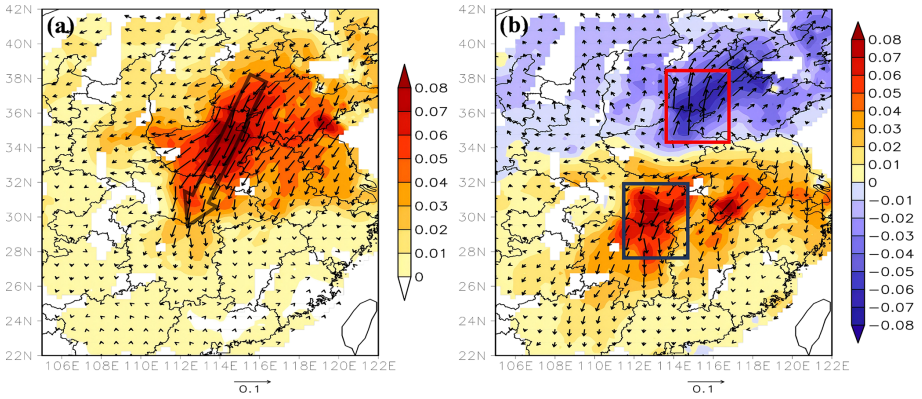

Figure 1. Spatial pattern of the **(a)** EOF1 and **(b)** EOF2 loads in the daily change of $PM_{2.5}$ TFV anomalies (vectors, unitless) and TFM anomalies (color contours, unitless) over CEC in the winters of 2015–2019. The red and blue boxes indicate the NCP and THB, respectively. The grid cells in white represent "missing values".

tion matrix is as follows:

$$X = \begin{bmatrix} x_{1,1}\cdots x_{1,n-5} \\ \vdots \\ x_{m,1}\cdots x_{m,n-5} \\ x_{1,2}\cdots x_{1,n-4} \\ \vdots \\ x_{m,2}\cdots x_{m,n-4} \\ x_{1,3}\cdots x_{1,n-3} \\ \vdots \\ x_{m,3}\cdots x_{m,n-3} \\ x_{1,4}\cdots x_{1,n-2} \\ \vdots \\ x_{m,4}\cdots x_{m,n-2} \\ x_{1,5}\cdots x_{1,n-1} \\ \vdots \\ x_{m,5}\cdots x_{m,n-1} \\ x_{1,6}\cdots x_{1,n} \\ \vdots \\ x_{m,6}\cdots x_{m,n} \end{bmatrix}. \quad (10)$$

Seen from Formula (10), the new extended matrix is composed of $X_{6m,n-5}$, where X is the $PM_{2.5}$ TFM anomalies, m is the spatial points of observation station, and n is the observation times of 450 d. When EEOF decomposition is performed on $PM_{2.5}$ TFV, the complex matrix is still used for the extension, and the same lag scheme is adopted to construct a new extended matrix of $PM_{2.5}$ TFV based on Formula (9). After constructing the initial data matrix, the EEOF decomposition method is in line with the classical EOF decomposition method.

Additionally, existing studies have utilized wavelet analysis, power spectrum analysis, and band-pass filtering methods to extract intraseasonal oscillation sequences of regional $PM_{2.5}$ concentrations (An et al., 2022; Gao et al., 2020; Li et al., 2021; Liu et al., 2022; Wu et al., 2023; Yang et al., 2024b). Such approaches may serve as alternative methods to EEOF analysis for establishing the quasi-weekly life cycle of regional $PM_{2.5}$ transport.

3 Results and discussion

3.1 QWO of regional $PM_{2.5}$ transport over CEC

The EOF decomposition is carried out on the daily anomalies of the $PM_{2.5}$ TFM and TFV in the winters of 2015–2019 over CEC. The first two EOFs explain 26.6 % and 14.2 % (29.1 % and 11.8 %) of the total anomalous variations in the $PM_{2.5}$ TFM (TFV), which is very helpful for better characterizing regional $PM_{2.5}$ transport variations.

Two principal modes govern the variations in $PM_{2.5}$ TF anomalies over CEC: the first leading monopole mode (EOF1) and the second meridional dipole mode (EOF2) (Fig. 1). EOF1 indicates the enhanced $PM_{2.5}$ TF over CEC (Fig. 1a). The large value center of TF mainly occurs in central China, and the transport vector direction is abnormally from the north to south. The horizontal $PM_{2.5}$ transport is unusually strong in central China, affected by the EAWM, presenting a typical channel for regional $PM_{2.5}$ transport over CEC (Yang et al., 2021a). The dipole mode of $PM_{2.5}$ TF anomalies displays a south–north out-of-phase pattern, with the flux large value centers located in the North China Plain (NCP) and the Twain-Hu Basin (THB), respectively, and the vector directions opposite (Fig. 1b). This mode indicates that the air pollutants from the NCP in the upwind region are transported to THB in the downwind region driven by the prevailing northerlies of the EAWM (Hu et al., 2021; Shen et al., 2022), and the $PM_{2.5}$ flux in NCP decreases, while that in THB increases in the regional $PM_{2.5}$ transport process.

Through EOF decomposition, the $PM_{2.5}$ TF could be understood from the perspective of a fixed time pattern of climate, but the temporal changes in the moving spatial struc-

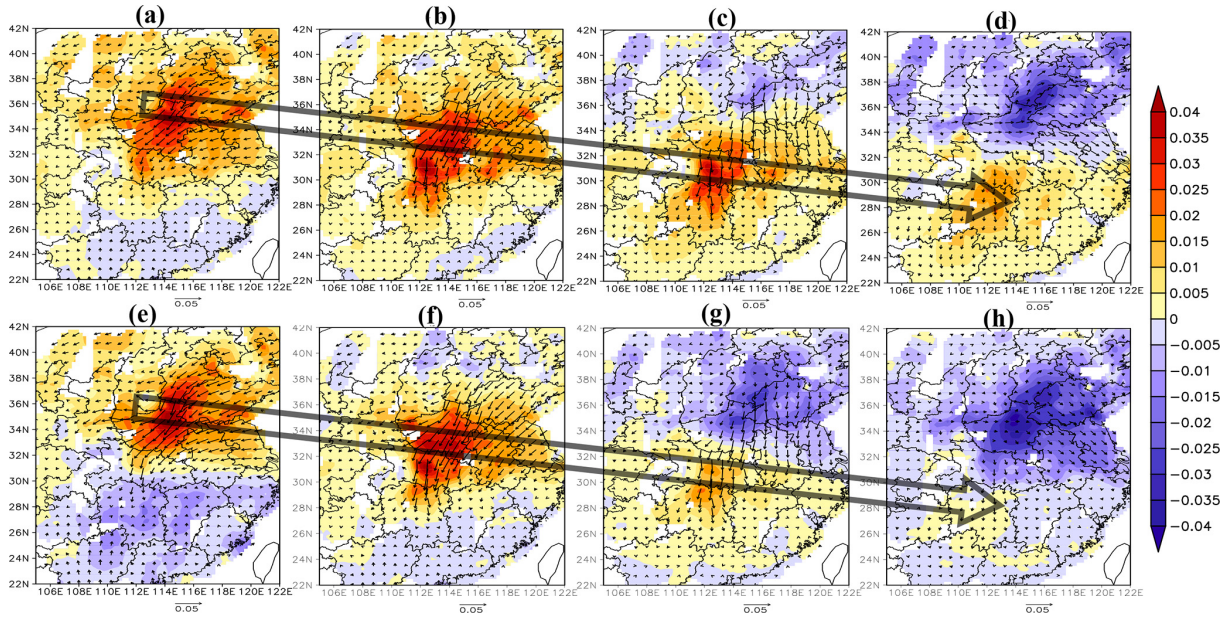

Figure 2. **(a–d)** The first four phases (days) of the QWO (8 d) during the regional $PM_{2.5}$ transport over CEC and **(e–h)** the first four phases (days) of the next cycle. The loads of $PM_{2.5}$ TFM anomalies (color contours, unitless) for EEOF2 and TFV anomalies (vectors, unitless) for EEOF1 with lag times of **(a)** 0 d, **(b)** 1 d, **(c)** 2 d, and **(d)** 3 d and loads of TFM anomalies (color contours, unitless) for EEOF3 and TFV anomalies (vectors, unitless) for EEOF2 with lag times of **(e)** 2 d, **(f)** 3 d, **(j)** 4 d, and **(h)** 5 d over CEC in the winters of 2015–2019.

ture of $PM_{2.5}$ TF over CEC failed to be obtained. However, EEOF decomposition can be used to analyze the continuous structural evolution of the main modes of regional $PM_{2.5}$ TF over CEC.

EEOF decomposition was carried out for the daily variations in $PM_{2.5}$ TFM anomalies and TFV anomalies, respectively, over CEC during the winters of 2015–2019. Figure 2 and Fig. S1 in the Supplement show the spatial distribution of different lag times for the main modes of EEOFs, which account for about 20 % of the total variation. According to the analysis, the $PM_{2.5}$ TFM anomalies for EEOF2 and EEOF3, as well as TFV anomalies for EEOF1 and EEOF2, all show the structural evolutions in the different phases of regional $PM_{2.5}$ transport in one cycle. As can be seen, Figs. 2a–d, S1a–d, and 2e–h describe the evolution of the first and second four phases in a cycle and the first four phases in the next cycle, respectively (one phase represents 1 d).

Figure 2a–d illustrate the positive anomalies of $PM_{2.5}$ TF shifting from the NCP to THB in the first four phases under the effect of the EAWM, causing the upwind $PM_{2.5}$ TF to decrease and the downwind $PM_{2.5}$ TF to increase, which is in line with the spatial pattern of the EOF modes in Fig. 1. The last four phases show the out-of-phase pattern of the first half cycle (Fig. S1a–d). It is noted that when anomalies of $PM_{2.5}$ TFV in the NCP turn to the northerly direction (Figs. S1d and 2e), it is a strong signal initiating the regional $PM_{2.5}$ transport. Then, the transport is repeated in the next periodic cycle (Fig. 2e–h). Therefore, the regional $PM_{2.5}$ transport over CEC shows a quasi-weekly (8 d) oscillation pattern.

To further study the variations in regional $PM_{2.5}$ transport over CEC, we have screened out 23 typical events with greater than 1.5 times standard deviations based on the standardized time coefficient of the EEOF and then used the 8 consecutive days of each event as the eight phases of the QWO in the composite analysis on the 23 typical events of regional $PM_{2.5}$ transport over CEC.

Figure 3 shows the composited $PM_{2.5}$ TF, divergence of $PM_{2.5}$ TF, and $PM_{2.5}$ concentration anomalies in the first four phases of the QWO. The high fluxes of $PM_{2.5}$ transport from north to south persist for 3–4 d over CEC and decline in the THB (Fig. 3a–d). The regional $PM_{2.5}$ transport lifetime corresponding to synoptic systems is about 3–5 d (Huang et al., 2020a). Abnormal northerly winds drive the heavy $PM_{2.5}$ pollution from the upwind NCP to the downwind regions, aggravating $PM_{2.5}$ pollution in the downwind THB (Fig. 3e–h). In the context of the QWO, the average $PM_{2.5}$ TFM in NCP decreases from approximately 400 $\mu g\,m^{-2}\,s^{-1}$ in the first and second phases to 200 and 100 $\mu g\,m^{-2}\,s^{-1}$ in the third and fourth phases, respectively (Fig. S2a). Correspondingly, the $PM_{2.5}$ concentration anomalies decline from around 100 $\mu g\,m^{-3}$ to approximately $-50\,\mu g\,m^{-3}$ (Fig. S2c). In the downwind THB, the average $PM_{2.5}$ TFM increases from about 200 $\mu g\,m^{-2}\,s^{-1}$ in the first phase to approximately 300 $\mu g\,m^{-2}\,s^{-1}$ in the second and third phases (Fig. S2b), with $PM_{2.5}$ concentration anomalies also rising to around 50 $\mu g\,m^{-3}$ (Fig. S2d).

It is noteworthy that the regions' $PM_{2.5}$ TF convergence zone (negative value of divergence) matches the positive

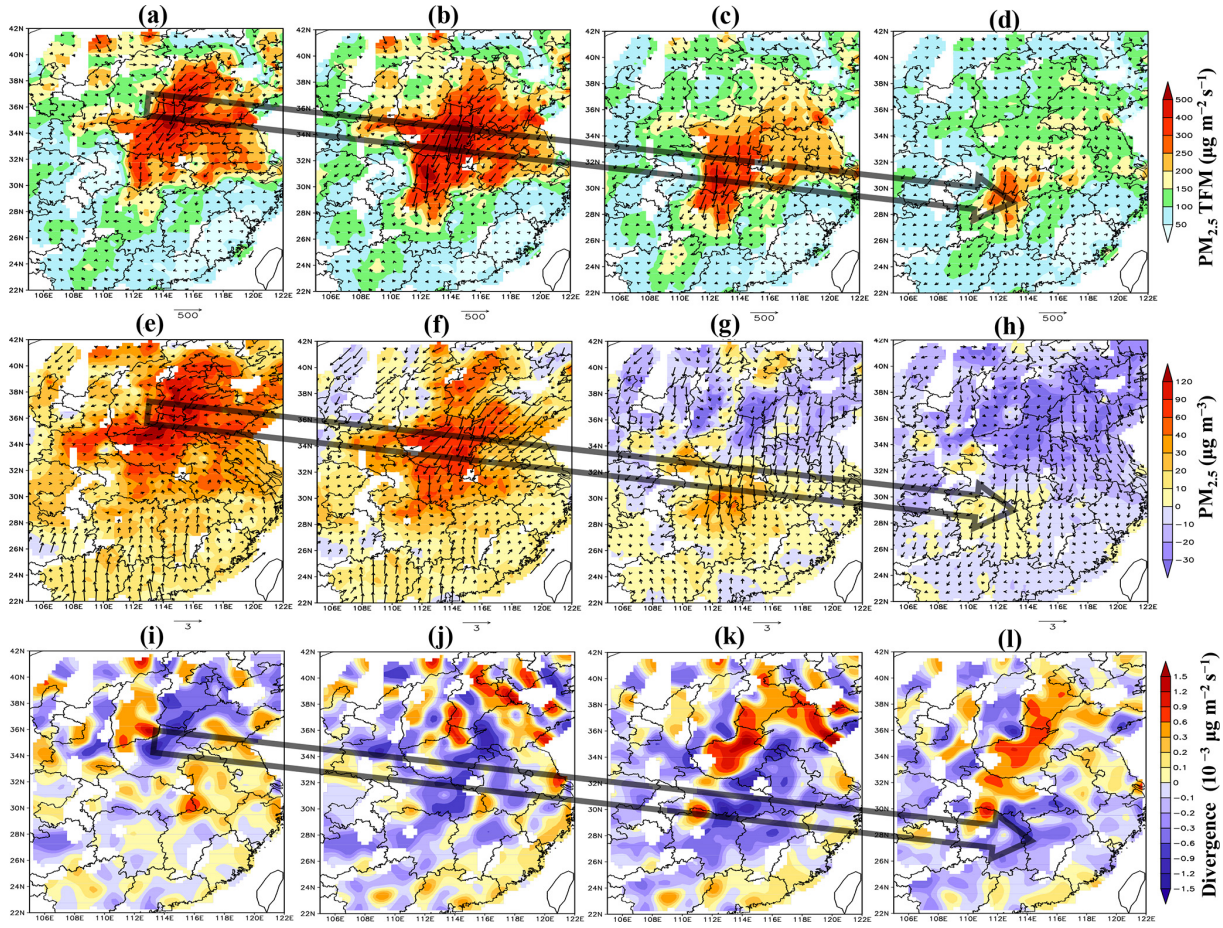

Figure 3. Spatial distributions of the composited **(a–d)** $PM_{2.5}$ TFM (color contours, unit: $\mu g\,m^{-2}\,s^{-1}$) and TFV (vectors, unit: $\mu g\,m^{-2}\,s^{-1}$), **(e–h)** anomalies of $PM_{2.5}$ concentrations (color contours, unit: $\mu g\,m^{-3}$) and 10 m wind vectors (unit: $m\,s^{-1}$), and **(i–l)** divergence of $PM_{2.5}$ flux (color contours, unit: $10^{-3}\,\mu g\,m^{-3}\,s^{-1}$) in the first four phases of the QWO during the 23 typical events of regional $PM_{2.5}$ transport over CEC.

anomaly centers of $PM_{2.5}$ concentrations spatially, which is confirmed with a significantly negative correlation of the $PM_{2.5}$ concentrations with divergence of $PM_{2.5}$ TF in the 23 typical events (Fig. S3). The $PM_{2.5}$ transport is accompanied by flux convergence, which is beneficial to the $PM_{2.5}$ accumulation. In addition, the $PM_{2.5}$ TF in the upwind NCP changes from convergence to divergence, and the divergence of the $PM_{2.5}$ TF in the downwind THB alters to convergence in the meantime (Fig. 3i–l), indicating that the $PM_{2.5}$ over THB is transported from the upwind NCP.

3.2 Source–receptor relationship in regional $PM_{2.5}$ transport from the NCP to THB

The regional pollutant transport governed by emissions and meteorology leads to a complex source–receptor relationship of air pollution changes (Yu et al., 2020). Band-pass filtering is performed on the daily $PM_{2.5}$ TFM anomalies at a quasi-weekly (6–9 d) synoptic scale in the winters of 2015–2019. In Fig. 4a, we composite the filter components of the $PM_{2.5}$ TFM in the eight phases of QWO during the 23 typical events of regional $PM_{2.5}$ transport over the NCP and THB, respectively. The $PM_{2.5}$ TF exhibits an obvious QWO on the synoptic scale (Fig. 4a). The $PM_{2.5}$ TF over the NCP continues to decline in the first four phases, while that of THB first rises and then falls in the last four phases, and the $PM_{2.5}$ TF over the NCP increases continuously, while that of THB falls first and then rises. We can see that the QWO of $PM_{2.5}$ TF over THB lags behind the NCP by two phases (Fig. 4a). The high TFM of $PM_{2.5}$ from the NCP in the first phase spread to THB, resulting in the peak of $PM_{2.5}$ TF over THB in the third phase.

In addition, the distribution of the differences in $PM_{2.5}$ TF and the vectors between phase 3 and phase 1 of the QWO and the $PM_{2.5}$ TF decrease and increase from phase 1 to phase 3, respectively, over the upwind NCP and the downwind THB, which is in accordance with the spatial pattern of the EOF mode (Figs. 1b and 4b), indicating the source–receptor rela-

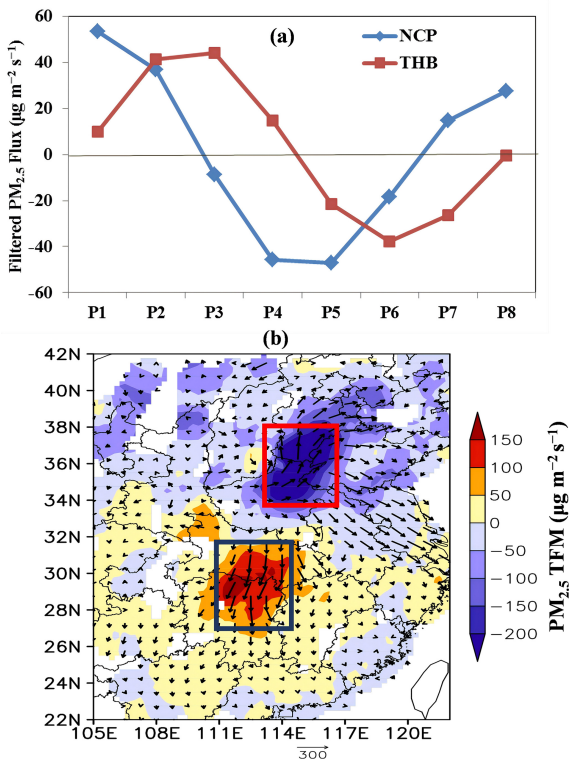

Figure 4. **(a)** The eight phases (P1–P8) of QWO during the 23 typical events of regional $PM_{2.5}$ transport over the NCP and THB with composited 6–9 d band-pass filtering of the $PM_{2.5}$ TFM and **(b)** spatial distribution of the differences in the $PM_{2.5}$ TFM (color contours, unit: $\mu g\,m^{-2}\,s^{-1}$) and TFV (vectors, unit: $\mu g\,m^{-2}\,s^{-1}$) between the third phase and the first phase of QWO. The red and black boxes represent the NCP and THB.

tionship in regional $PM_{2.5}$ transport from the NCP to THB over CEC.

The statistical analysis based on long-term observation also shows that there is a significant 2 d lag relationship of positive correlation between the NCP and THB in $PM_{2.5}$ TF in the QWO (Fig. 5a). This shows that the air pollutants are transported from the upwind NCP to the downwind THB in 2 d, confirming a quasi-2 d lag in the regional $PM_{2.5}$ transport from the NCP to THB (Hu et al., 2021; Shen et al., 2021). Additionally, in the long-term change of air pollution, the divergences of $PM_{2.5}$ TF in the NCP are significantly negatively correlated to that of THB (Fig. 5b); that is, the $PM_{2.5}$ TF convergence in the downwind THB fits well with the $PM_{2.5}$ TF divergence in the upwind NCP. It can be reflected that the changes in the synoptic scale of the EAWM atmospheric circulation cause the regional $PM_{2.5}$ transport to build the source–receptor relationship of atmospheric pollutants between the NCP and THB.

Driven by prevailing winds of the EAWM, the THB became the main receptor for regional transport of air pollutants over CEC (Bai et al., 2022; Shen et al., 2021). During 2015–2019, approximately 65.2 % of the total $PM_{2.5}$ heavy pollution events in the THB were triggered by regional transport of air pollutants over CEC (Hu et al., 2022; Shen et al., 2021). Such $PM_{2.5}$ transport from upstream source regions in CEC contributes 51 %–85.7 % of the $PM_{2.5}$ pollution over the THB receptor region (Hu et al., 2021; Lu et al., 2017; Shen et al., 2022; Yu et al., 2020), revealing the dominance of regional transport of air pollutants from CEC to the THB with the meteorological drivers. Our research emphasizes the QWO of regional $PM_{2.5}$ transport over CEC with the driver of the synoptic-scale disturbances of the EAWM circulation, confirming the source–receptor relationships with their 2 d lagging effects in the regional $PM_{2.5}$ transport between the upstream NCP source region and the THB receptor region.

3.3 Effect of synoptic-scale disturbance of the EAWM circulation on QWO of regional $PM_{2.5}$ transport over CEC

Meteorological change is the essential factor in regulating the occurrence and development of $PM_{2.5}$ pollution on synoptic scales. To investigate the QWO of the EAWM circulation in the synoptic-scale disturbance, this study performs the 6–9 d band-pass filtering of the daily SLP anomalies (denoted as SLP_{QWO}) in East Asia during the winters of 2015–2019. The SLP and SLP_{QWO} fields (Figs. 6 and 7) as well as $PM_{2.5}$ concentrations and 10 m winds (Fig. S4) in the eight phases of QWO during the 23 typical events were composited, respectively. The QWO of regional $PM_{2.5}$ transport is connected with the "weekly cycle" synoptic process of $PM_{2.5}$ transport and accumulation over CEC (Fig. S4), and it is powered mainly by the Siberian high circulation with the synoptic-scale disturbance of the EAWM circulation (Figs. 6 and 7).

The condition of uniform pressure in the front of the Siberian high could favor the $PM_{2.5}$ accumulation over the NCP for triggering regional $PM_{2.5}$ transport over CEC (Fig. 7a). The regional heavy pollution of $PM_{2.5} > 150\,\mu g\,m^{-3}$ lasts for 1–2 d (Fig. S4a and b). With the development of the Siberian high, the extension of the high pressure guides the cold air to advance southward (Park et al., 2014). As the result of the increasing air pressure gradients, the strong northerly winds in the EAWM circulation system deliver high-level $PM_{2.5}$ air mass from the NCP to THB (Figs. 7a–d, S4a–d). In addition, the cold and high air pressure system with the abnormal northerly airflows moves from the Siberia–Mongolia region to CEC in the first four phases (Fig. 6), providing beneficial synoptic circulation patterns for regional $PM_{2.5}$ transport. Thus, the periodic extension of the Siberian high with the associated strong cold-air intrusion is an important driver in the regional $PM_{2.5}$ transport over CEC.

Notably, we can see that in the first four phases, the SLP_{QWO} positive anomalies occur, develop, and expand southward from the Siberia–Mongolia region to CEC (Fig. 7a–d). The synoptic-scale disturbance with the exten-

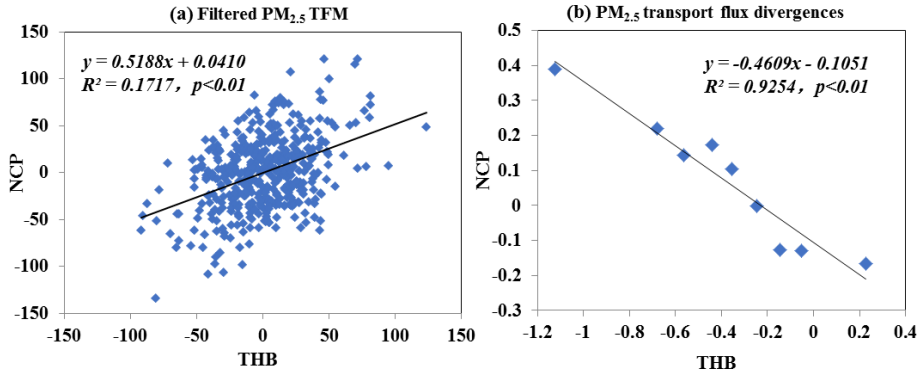

Figure 5. **(a)** Scatter plot of 6–9 d filtering components of the $PM_{2.5}$ TFM (10^{-3} μg m^{-2} s^{-1}) over THB in 2 d lag and the NCP during the winters of 2015–2019 and **(b)** scatter plot of $PM_{2.5}$ TF divergences (10^{-3}μg m^{-3} s^{-1}) between THB and the NCP; the $PM_{2.5}$ TF divergences are averaged over the value interval of 0.1.

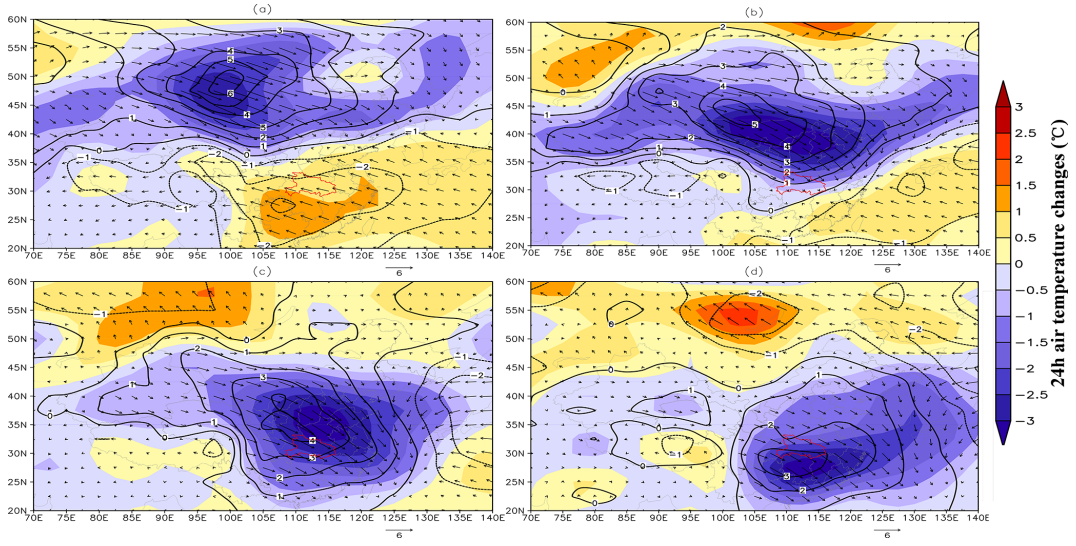

Figure 6. The composited differences between the current day and the previous day of SLP (black contour lines, unit: hPa), 1000 hPa air temperature (color contours, unit: °C), and wind vectors (unit: m s^{-1}) in the first four phases **(a–d)** of QWO during the 23 typical events.

sion of the Siberian high and the southward movement of cold air could drive the regional $PM_{2.5}$ transport over CEC (Fig. 7a–d). The situation of the last four phases is opposite to the SLP_{QWO} negative anomalies in Siberia–Mongolia region, inhibiting the Siberian high and cold-air intrusion (Fig. 7e–h). The low and uniform pressure is beneficial to the accumulation of $PM_{2.5}$. Therefore, the periodic changes in the synoptic-scale disturbance of the EAWM circulation cause the QWO of regional $PM_{2.5}$ transport over CEC.

In addition, EEOF decomposition is carried out on the SLP_{QWO} field in the winters of 2015–2019 to recognize the periodic activities in the synoptic scale of the EAWM circulation. The cold-air activity of the EAWM presents QWO (Wu and Wang, 2002). The positive (negative) synoptic-scale disturbance occurs in the Siberia–Mongolia region and then spreads to CEC along the northwest–southeast path, contributing to the 8 d cycle of QWO (Fig. S5). Notably, the spatial correlation coefficients between the load of SLP_{QWO} decomposed by the EEOF (Fig. S5) and the SLP_{QWO} composited during 23 typical events (Fig. 7) are highly positively correlated in the eight phases. Therefore, the QWO in the synoptic-scale activities of the Siberian high is an important factor for driving the QWO of regional $PM_{2.5}$ transport over CEC.

4 Conclusions

Exploring the periodical oscillations of $PM_{2.5}$ pollution over CEC and the meteorological effect is crucial for understanding the change in the atmospheric environment and improving regional air quality forecasts. In this study that constructed a dataset of the daily $PM_{2.5}$ TF, the EEOF and statistical methods are used to identify the QWO of regional $PM_{2.5}$ transport with the spatiotemporal variations over CEC

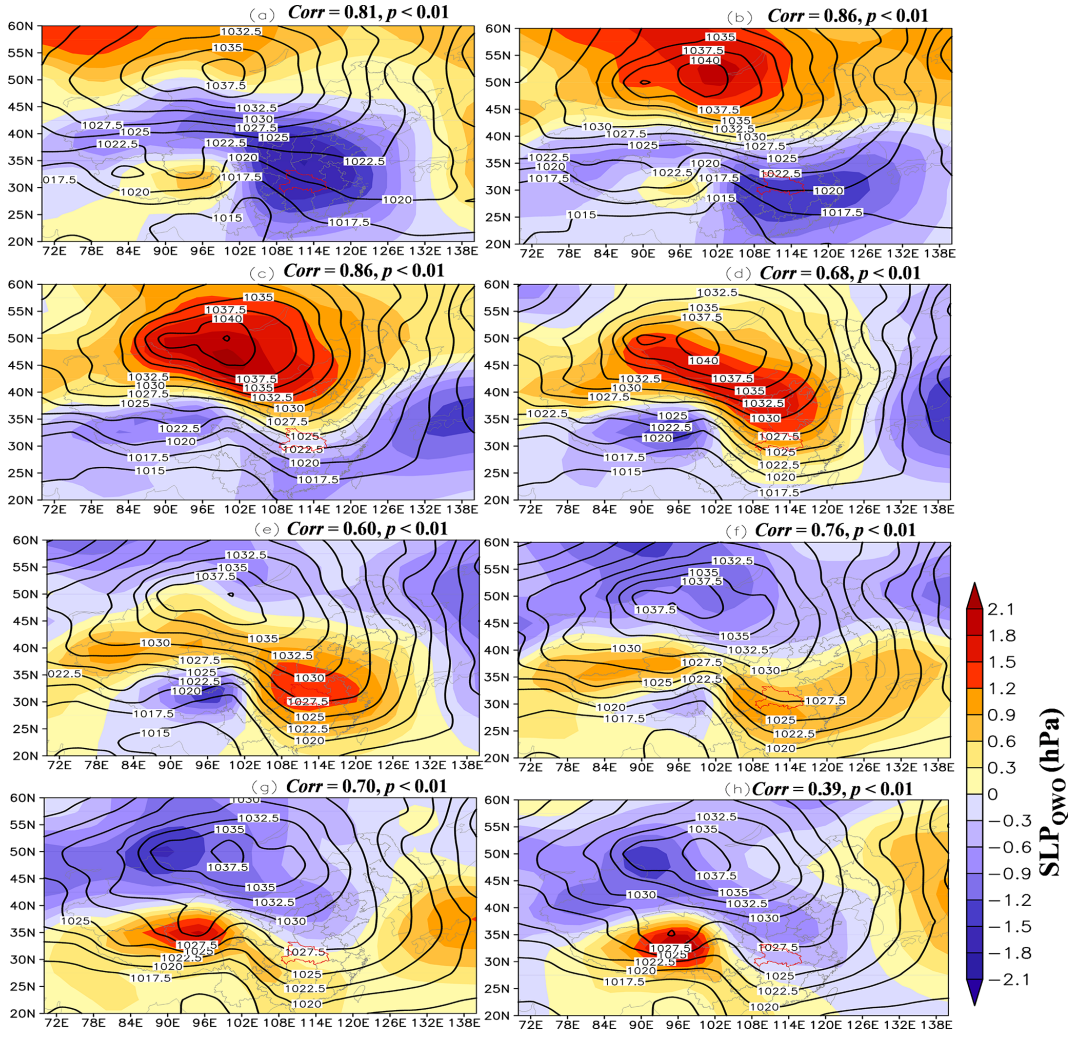

Figure 7. Composited SLP (black contour lines, unit: hPa) and its synoptic-scale filter component SLP_{QWO} (color contours, unit: hPa) in the eight phases **(a–h)** of QWO during the 23 typical events. *Corr* represents the spatial correlation coefficients between SLP_{QWO} and the load of SLP_{QWO} decomposed by the EEOF in Fig. S4.

in winters from 2015 to 2019. The source–receptor relationship is recognized between NCP and THB with the QWO of regional $PM_{2.5}$ transport over CEC with the typical EAWM climate. Furthermore, the driving effect of synoptic-scale disturbance of the EAWM circulation on the QWO of regional $PM_{2.5}$ transport over China is revealed.

The variations in $PM_{2.5}$ TF over CEC are dominated by the first leading monopole mode and the second meridional dipole mode. The monopole mode indicates the high $PM_{2.5}$ flux along the channel of regional $PM_{2.5}$ transport from the NCP to THB under the EAWM circulation, and the dipole mode exhibits a south–north out-of-phase pattern, with two centers existing, respectively, in the upwind NCP and the downwind THB in regional transport of $PM_{2.5}$ over CEC. In terms of the long-term changes in air pollution of 2015–2019, the regional $PM_{2.5}$ transport over CEC is confirmed by the QWO, verifying a source–receptor relationship for the regional $PM_{2.5}$ transport from the NCP to THB in 2 d. Such changes are incurred by the QWO in the activities of the Siberian high, and this synoptic-scale disturbance of the EAWM circulation is generated in the Siberia–Mongolia region and then develops, moving into CEC, regulating the QWO of regional $PM_{2.5}$ transport.

The EEOF analysis with the temporal lag of the spatial fields is able to better characterize the spatial and temporal evolution of perturbations, especially propagating waves in the atmosphere (Weare and Nasstrom, 1982; Qian et al., 2019; Yang et al., 2024b). Due to its technical advantages, the EEOF method is commonly employed to extract atmospheric oscillation patterns to reveal the impacts and mechanisms of atmospheric fluctuations and monsoon circulation on regional weather, climate, and atmospheric environments (Dey et al., 2018; Qian et al., 2019; Yang et al., 2024b). In this study, we employed the EEOF method to identify re-

gional $PM_{2.5}$ transport modes on a synoptic scale, by constructing the $PM_{2.5}$ transport flux vector (TFV) and the transport flux magnitude (TFM) with the product of near-surface $PM_{2.5}$ concentrations and wind components at 1079 stations across China during the winters of 2015–2019. We performed EEOF analysis on the $PM_{2.5}$ TFV and TFM, resulting in the spatial structure of $PM_{2.5}$ transport flux under the temporal disturbances at the synoptic scale and revealing the connection between synoptic-scale disturbances in the EAWM and QWO in regional $PM_{2.5}$ transport in CEC. Our study focuses on the driving effects of synoptic-scale disturbances associated with cold-air activity with the anomalous northerly winds in EAWM on QWO of regional $PM_{2.5}$ transport over CEC, exacerbating $PM_{2.5}$ pollution in the downwind THB. Differently from the studies on stagnant meteorological conditions associated with $PM_{2.5}$ accumulations (Gao et al., 2020; Wu et al., 2023; Yang et al., 2024b), this study provides new insights into the understanding of regional $PM_{2.5}$ transport with the source–receptor relationship and the meteorological mechanism in atmospheric environment change.

Based on the five-winter (2015–2019) observations of $PM_{2.5}$ concentrations and the corresponding meteorological reanalysis data, this study with the climate statistical and diagnostic methods investigates the QWO of regional $PM_{2.5}$ transport in China with the influence of synoptic-scale disturbance of the EAWM circulation, providing new insight into the understanding of regional air pollutant transport with meteorological drivers in atmospheric environment changes. Besides the EEOF method used in this study, the alternative methods of wavelet analysis, power spectrum analysis, and band-pass filtering could be used in further study. Future studies with utilizing long-term observations of air pollutants and meteorology over CEC could more comprehensively understand the variations in the regional transport of particles and the gaseous precursors with their contributions to air pollution, through the integration of artificial intelligence and physical–chemical process analyses.

Data availability. The $PM_{2.5}$ concentrations were obtained from https://quotsoft.net/air/ (Wang, 2025). The ERA5-Land reanalysis is available at https://doi.org/10.24381/cds.e2161bac (Muñoz Sabater, 2019). The NCEP/NCAR reanalysis is available at https://psl.noaa.gov/data/gridded/tables/daily.html (NOAA, 2025). All data used in this paper can be provided upon request from Yongqing Bai (2007byq@163.com).

Supplement. The supplement related to this article is available online at: https://doi.org/10.5194/acp-25-1273-2025-supplement.

Author contributions. YB and TZ conceived the study. YB designed the graphics and wrote the manuscript with help from TZ, and KM, YZ, JX, XS, LS, YY, YZ, WH, and JY were involved in the scientific discussion. All authors commented on the paper.

Competing interests. The contact author has declared that none of the authors has any competing interests.

Disclaimer. Publisher's note: Copernicus Publications remains neutral with regard to jurisdictional claims made in the text, published maps, institutional affiliations, or any other geographical representation in this paper. While Copernicus Publications makes every effort to include appropriate place names, the final responsibility lies with the authors.

Financial support. This research has been supported by the National Natural Science Foundation of China (grant nos. 42075186 and 41830965) and the National Key Research and Development Program of China (2022YFC3701204).

Review statement. This paper was edited by Zhonghua Zheng and reviewed by I. Pérez and two anonymous referees.

References

An, X., Chen, W., Hu, P., Chen, S., and Sheng, L.: Intraseasonal variation of the northeast Asian anomalous anticyclone and its impacts on $PM_{2.5}$ pollution in the North China Plain in early winter, Atmos. Chem. Phys., 22, 6507–6521, https://doi.org/10.5194/acp-22-6507-2022, 2022.

An, Z., Huang, R., Zhang, R., Tie, X., Li, G., Cao, J., Zhou, W., Shi, Z., Han, Y., Gu, Z., and Ji, Y.: Severe haze in northern China: A synergy of anthropogenic emissions and atmospheric processes, P. Natl. Acad. Sci. USA, 116, 8657–8666, https://doi.org/10.1073/pnas.1900125116, 2019.

Bai, Y., Zhao, T., Zhou, Y., Kong, S., Hu, W., Xiong, J., Liu, L., Zheng, H., and Meng, K.: Aggravation effect of regional transport on wintertime $PM_{2.5}$ over the middle reaches of the Yangtze River under China's air pollutant emission reduction process, Atmos. Pollut. Res., 12, 101111, https://doi.org/10.1016/j.apr.2021.101111, 2021.

Bai, Y., Zhao, T., Hu, W., Zhou, Y., Xiong, J., Wang, Y., Liu, L., Shen, L., Kong, S., Meng, K., and Zheng, H.: Meteorological mechanism of regional $PM_{2.5}$ transport building a receptor region for heavy air pollution over Central China, Sci. Total Environ., 808, 151951, https://doi.org/10.1016/j.scitotenv.2021.151951, 2022.

Bäumer, D. and Vogel, B.: An unexpected pattern of distinct weekly periodicities in climatological variables in Germany, Geophys. Res. Lett., 34, L03819, https://doi.org/10.1029/2006gl028559, 2007.

Cai, W., Li, K., Liao, H., Wang, H., and Wu, L.: Weather conditions conducive to Beijing severe haze more frequent under climate change, Nat. Clim. Change, 7, 257–262, https://doi.org/10.1038/nclimate3249, 2017.

Chen, X., Yin, L., Fan Y., Song, L., Ji, T., Liu, Y., Tian, J., and Zheng, W.: Temporal evolution characteristics of $PM_{2.5}$ concentration based on continuous wavelet transform, Sci. Total Environ., 699, 134244, https://doi.org/10.1016/j.scitotenv.2019.134244, 2020.

Chin, M.: Dirtier air from a weaker monsoon, Nat. Geosci., 5, 449–450, https://doi.org/10.1038/ngeo1513, 2012.

Compo, G. P., Kiladis, G. N., and Webster, P. J.: The horizontal and vertical structure of east Asian winter monsoon pressure surges, Q. J. Roy. Meteor. Soc., 125, 29–54, https://doi.org/10.1256/smsqj.55302, 1999.

Dey, A., Chattopadhyay, R., Sahai, A. K., Mandal, R., Joseph, S., Phani, R., and Abhilash, S.: An operational tracking method for the MJO using extended empirical orthogonal functions, Pure. Appl. Geophys., 176, 2697–2717, https://doi.org/10.1007/s00024-018-2066-8, 2018.

Ding, A., Huang, X., and Fu, C.: Air Pollution and Weather Interaction in East Asia, Oxford Research Encyclopedia-Environmental Science, https://doi.org/10.1093/acrefore/9780199389414.013.536, 2017.

Dong, Y., Zhou, H., Fu, Y., Li, X., and Geng, H.: Wavelet periodic and compositional characteristics of atmospheric $PM_{2.5}$ in a typical air pollution event at Jinzhong city, China, Atmos. Pollut. Res., 12, 245–254, https://doi.org/10.1016/j.apr.2020.09.013, 2021.

Fan, J., Wang, Y., Rosenfeld, D., and Liu, X.: Review of aerosol–cloud interactions: Mechanisms, significance, and challenges, J. Atmos. Sci., 73, 4221–4252, https://doi.org/10.1175/jas-d-16-0037.1, 2016.

Feng, J., Zhu, J., Li, J., and Liao, H.: Aerosol concentrations variability over China: two distinct leading modes, Atmos. Chem. Phys., 20, 9883–9893, https://doi.org/10.5194/acp-20-9883-2020, 2020.

Fu, H., Zhang, Y., Liao C., Mao, L., Wang, Z., and Hong, N.: Investigating $PM_{2.5}$ responses to other air pollutants and meteorological factors across multiple temporal scales, Sci. Rep., 10, 15639, https://doi.org/10.1038/s41598-020-72722-z , 2020.

Gao, L., Wang, T., Ren X., Zhuang, B., Li, S., Yao, R., and Yang, X.: Impact of atmospheric quasi-biweekly oscillation on the persistent heavy $PM_{2.5}$ pollution over Beijing-Tianjin-Hebei region, China during winter, Atmos. Res., 242, 105017, https://doi.org/10.1016/j.atmosres.2020.105017, 2020.

Ge, B., Wang, Z., Lin, W., Xu, X., Li, J., Ji, D., and Ma, Z.: Air pollution over the North China Plain and its implication of regional transport: A new sight from the observed evidences, Environ. Pollut., 234, 29–38, https://doi.org/10.1016/j.envpol.2017.10.084, 2018.

Geng, G., Zheng, Y., Zhang Q., Xue, T., Zhao, H., Tong, D., Zheng, B., Li, M., Liu, F., Hong, C., He, K., and Davis, S. J.: Drivers of $PM_{2.5}$ air pollution deaths in China 2002–2017, Nat. Geosci., 14, 645–650, https://doi.org/10.1038/s41561-021-00792-3, 2021.

Georgoulias, A. K. and Kourtidis, K. A.: A high resolution satellite view of the aerosol weekly cycle variability over Central Europe, Atmos. Res., 107, 145–160, https://doi.org/10.1016/j.atmosres.2012.01.003, 2012.

Gouirand, I., Jury, M. R., and Sing, B.: An analysis of low- and high-frequency summer climate variability around the Caribbean Antilles, J. Climate, 25, 3942–3952, https://doi.org/10.1175/jcli-d-11-00269.1, 2012.

Guo, S., Hu, M., Zamora, M. L., Peng, J., and Zhang, R.: Elucidating severe urban haze formation in China, P. Natl. Acad. Sci. USA, 111, 17373–17378, https://doi.org/10.1073/pnas.1419604111, 2014.

Hou, X., Zhu, B., Kumar, K. R., de Leeuw, G., Lu, W., Huang, Q., and Zhu, X.: Establishment of conceptual schemas of surface synoptic meteorological situations affecting fine particulate pollution across eastern China in the winter, J. Geophys. Res.-Atmos., 125, e2020JD033153, https://doi.org/10.1029/2020jd033153, 2020.

Hu, W., Zhao, T., Bai, Y., Kong, S., Xiong, J., Sun, X., Yang, Q., Gu, Y., and Lu, H.: Importance of regional $PM_{2.5}$ transport and precipitation washout in heavy air pollution in the Twain-Hu Basin over Central China: Observational analysis and WRF-Chem simulation, Sci. Total Environ., 758, 143710, https://doi.org/10.1016/j.scitotenv.2020.143710, 2021.

Hu, W., Zhao, T., Bai, Y., Kong, S., Shen, L., Xiong, J., Zhou, Y., Gu, Y., Shi, J., Zheng, H., Sun, X., and Meng, K.: Regulation of synoptic circulation in regional $PM_{2.5}$ transport for heavy air pollution: Study of 5-year observation over central China, J. Geophys. Res.-Atmos., 127, e2021JD035937, https://doi.org/10.1029/2021JD035937, 2022.

Huang, H., Wang, S., Huang, W., Lin, N., Chuang, M., Silva, A. M., and Peng. C.: Influence of synoptic-dynamic meteorology on the long-range transport of Indochin biomass burning aerosols, J. Geophys. Res.-Atmos., 125, e2019JD031260, https://doi.org/10.1029/2019jd031260, 2020a.

Huang, R. J., Zhang, Y., Bozzetti, C., Ho, K. F., Cao, J. J., Han, Y., Daellenbach. K. R., Slowik, J. G., Platt, S. M., Canonaco, F., Zotter, P., Wolf, R., Pieber, S. M., Bruns, E., A., Crippa, M., Ciarelli, G., Piazzalunga, A., Schwikowski. M., Abbaszade, G., Kreis, J. S., Zimmermann, R., An, Z., Szidat, S., Baltensperger, U., Haddad, I. E., and Prevot, A. S. H.: High secondary aerosol contribution to particulate pollution during haze events in China, Nature, 514, 218–222, https://doi.org/10.1038/nature13774, 2014.

Huang, X., Wang, Z., and Ding, A.: Impact of aerosol-PBL interaction on haze pollution: Multiyear observational evidences in North China, Geophys. Res. Lett., 45, 8596–8603, https://doi.org/10.1029/2018gl079239, 2018.

Huang, X., Ding, A., Wang, Z., Ding, K., Gao, J., Chai, F., and Fu, C.: Amplified transboundary transport of haze by aerosol–boundary layer interaction in china, Nat. Geosci., 13, 428–434, https://doi.org/10.1038/s41561-020-0583-4, 2020b.

Jia, B., Wang, Y., Yao, Y., and Xie, Y.: A new indicator on the impact of large-scale circulation on wintertime particulate matter pollution over China, Atmos. Chem. Phys., 15, 11919–11929, https://doi.org/10.5194/acp-15-11919-2015, 2015.

Kang, H., Zhu, B., Gao, J., He, Y., Wang, H., Su, J., Pan, C., Zhu, T., and Yu, B.: Potential impacts of cold frontal passage on air quality over the Yangtze River Delta, China, Atmos. Chem. Phys., 19, 3673–3685, https://doi.org/10.5194/acp-19-3673-2019, 2019.

Kim, B. H. and Ha, K. J.: Observed changes of global and western Pacific precipitation associated with global warming SST mode and mega-ENSO SST mode, Clim. Dynam., 45, 3067–3075, https://doi.org/10.1007/s00382-015-2524-2, 2015.

Li, Q., Zhang, R., and Wang, Y.: Interannual variation of the wintertime fog-haze days across central and eastern China

and its relation with EAWM, Int. J. Climatol., 36, 346–354, https://doi.org/10.1002/joc.4350, 2016.

Li, X., Gereon, G., Greatbatch, R. J., and Lu, R.: Impact of the MJO on the interannual variation of the Pacific–Japan mode of the East Asian summer monsoon, Clim. Dynam., 52, 3489–3501, https://doi.org/10.1007/s00382-018-4328-7, 2019.

Li, X., Yu, C., Deng, X., He, D., Zhao, Z., Mo, H., Mo, J., and Wu, Y.: Mechanism for synoptic and intra-seasonal oscillation of visibility in Beijing-Tianjin-Hebei region, Theor. Appl. Climatol., 143, 1005–1015, https://doi.org/10.1007/s00704-020-03466-z, 2021.

Lin, Y., Zou, J., Yang, W., and Li, C. Q.: A Review of Recent Advances in Research on $PM_{2.5}$ in China, Int. J. Env. Res. Pub. He., 15, 438, https://doi.org/10.3390/ijerph15030438, 2018.

Liu, J., Mauzerall, D. L., Chen, Q., Zhang, Q., Song, Y, Peng, W., Klimont. Z., Qiu, X., Zhang, S., Hu, M., Lin, W., Smith, K. R., and Zhu, T.: Air pollutant emissions from Chinese households: A major and underappreciated ambient pollution sources, P. Natl. Acad. Sci. USA, 113, 7756–7761, https://doi.org/10.1073/pnas.1604537113, 2016.

Liu, J., Huang, W., and Zhang, Q.: The quasi-biweekly oscillation of eastern China $PM_{2.5}$ in response to different Rossby wave trains over the Eurasian continent, Atmos. Res., 267, 105990, https://doi.org/10.1016/j.atmosres.2021.105990, 2022.

Liu, Q., Jia, X., Quan, J., Li, J., Li, X., Wu, Y., Chen, D., Wang, Z., and Liu, Y.: New positive feedback mechanism between boundary layer meteorology and secondary aerosol formation during severe haze events, Sci. Rep., 8, 6095, https://doi.org/10.1038/s41598-018-24366-3, 2018.

Liu, Y., Tang, G., Zhou, L., Hu, B., Liu, B., Li, Y., Liu, S., and Wang, Y.: Mixing layer transport flux of particulate matter in Beijing, China, Atmos. Chem. Phys., 19, 9531–9540, https://doi.org/10.5194/acp-19-9531-2019, 2019.

Lu, M., Tang, X., Wang, Z., Gbaguidi, A., Liang, S., Hu, K., Wu, L., Wu, H., Huang, Z., and Shen, L.: Source tagging modeling study of heavy haze episodes under complex regional transport processes over Wuhan megacity, Central China, Environ. Pollut., 231, 612–621, https://doi.org/10.1016/j.envpol.2017.08.046, 2017.

Ma, Y., Zhu, Y., Liu, B., Li, H., Jin, S., Zhang, Y., Fan, R., and Gong, W.: Estimation of the vertical distribution of particle matter ($PM_{2.5}$) concentration and its transport flux from lidar measurements based on machine learning algorithms, Atmos. Chem. Phys., 21, 17003–17016, https://doi.org/10.5194/acp-21-17003-2021, 2021.

Merrill, J. T. and Kim, J.: Meteorological events and transport patterns in ACE-Asia, J. Geophys. Res.-Atmos., 109, D19S18, https://doi.org/10.1029/2003jd004124, 2004.

Miao, Y., Hu, X. M., Liu, S., Qian, T., Xue, M., Zheng, Y., and Wang, S.: Seasonal variation of local atmospheric circulations and boundary layer structure in the Beijing-Tianjin-Hebei region and implications for air quality, J. Adv. Model. Earth Sy., 7, 1602–1626, 2015.

Miao, Y., Li, J., Miao, S., Che, H., Wang, Y., Zhang, X., Zhu, R., and Liu, S.: Interaction between planetary boundary layer and $PM_{2.5}$ pollution in megacities in China: a review, Curr. Pollut. Rep., 5, 261–271, https://doi.org/10.1002/2015ms000522, 2019.

Muñoz Sabater, J.: ERA5-Land hourly data from 1950 to present, Copernicus Climate Change Service (C3S) Climate Data Store (CDS) [data set], https://doi.org/10.24381/cds.e2161bac, 2019.

Murakami, T.: Winter monsoonal surges over East and Southeast Asia, J. Meteor. Soc. Jpn., 57, 133–158, https://doi.org/10.2151/jmsj1965.57.2_133, 1979.

Nie, W., Ding, A., Wang, T., Kerminen, V. M., George, C., Xue, L., Wang, W., Zhang, Q., Petäjä, T., Qi, X., Gao, X., Wang, X., Yang, X., Fu, C., and Kulmala, M.: Polluted dust promotes new particle formation and growth, Sci. Rep., 4, 6634, https://doi.org/10.1038/srep06634, 2014.

NOAA: Gridded Climate Datasets, https://psl.noaa.gov/data/gridded/tables/daily.html, last access: 27 January 2025.

Park, T. W., Ho, C. H., and Deng, Y.: A synoptic and dynamical characterization of wave-train and blocking cold surge over East Asia, Clim. Dynam., 43, 753–770, https://doi.org/10.1007/s00382-013-1817-6, 2014.

Perrone, M. R., Vecchi, R., Romano, S., Becagli, S., Traversi, R., and Paladini, F.: Weekly cycle assessment of PM mass concentrations and sources, and impacts on temperature and wind speed in Southern Italy, Atmos. Res., 218, 129–144, https://doi.org/10.1016/j.atmosres.2018.11.013, 2018.

Qian, Y., Hsu, P. C., and Kazuyoshi, K.: New real-time indices for the quasi-biweekly oscillation over the Asian summer monsoon region, Clim. Dynam., 53, 2603–2624, https://doi.org/10.1007/s00382-019-04644-0, 2019.

Quan, J., Tie, X., Zhang, Q., Liu, Q., Li, X., Gao,Y., and Zhao, D.: Characteristics of heavy aerosol pollution during the 2012–2013 winter in Beijing, China, Atmos. Environ., 88, 83–89, https://doi.org/10.1016/j.atmosenv.2014.01.058, 2014.

Quan, J., Xu, X., Jia, X.. Liu, S., Miao, S., Xin, J., Hu, F., Wang, Z., Fan, S., Zhang, H., Mu, Y., Dou, Y., and Cheng, Z.: Multi-scale processes in severe haze events in China and their interactions with aerosols: Mechanisms and progresses, Chin. Sci. Bull., 65, 810–824, https://doi.org/10.1360/tb-2019-0197, 2020.

Schepanski, K., Mallet, M., Heinold, B., and Ulrich, M.: North African dust transport toward the western Mediterranean basin: atmospheric controls on dust source activation and transport pathways during June–July 2013, Atmos. Chem. Phys., 16, 14147–14168, https://doi.org/10.5194/acp-16-14147-2016, 2016.

Shen, L., Hu, W., Zhao, T., Bai, Y., Wang, H., Kong, S., and Zhu, Y.: Changes in the Distribution Pattern of $PM_{2.5}$ Pollution over Central China, Remote. Sens., 13, 4855, https://doi.org/10.3390/rs13234855, 2021.

Shen, L., Zhao, T., Liu, J., Wang, H., Bai, Y., Kong, S., and Shu, Z.: Regional transport patterns for heavy $PM_{2.5}$ pollution driven by strong cold airflows in Twain-Hu Basin, Central China, Atmos. Environ., 269, 118847, https://doi.org/10.1016/j.atmosenv.2021.118847, 2022.

Shu, Z., Liu, Y., Zhao, T., Xia, J., Wang, C., Cao, L., Wang, H., Zhang, L., Zheng, Y., Shen, L., Luo, L., and Li, Y.: Elevated 3D structures of $PM_{2.5}$ and impact of complex terrain-forcing circulations on heavy haze pollution over Sichuan Basin, China, Atmos. Chem. Phys., 21, 9253–9268, https://doi.org/10.5194/acp-21-9253-2021, 2021.

Tan, Q., Ge, B., Xu, X., Gan, L., Yang, W., Chen, X., Pan, X., Wang, W., Li, J., and Wang, Z.: Increasing impacts of the relative contributions of regional transport on air pollution in

Beijing: Observational evidence, Environ. Pollut., 292, 118407, https://doi.org/10.1016/j.envpol.2021.118407, 2021.

Tao, M., Chen, L., Li, R., Wang, L., Wang, J., Wang, Z., Tang, G., and Tao, J.: Spatial oscillation of the particle pollution in eastern China during winter: Implications for regional air quality and climate, Atmos. Environ., 144, 100–110, https://doi.org/10.1016/j.atmosenv.2016.08.049, 2016.

Wang, H., Kumar, A., Murtugudde, R., Narapusetty, B., and Seip, K. L.: Covariations between the Indian Ocean dipole and ENSO: a modeling study, Clim. Dynam., 53, 5743–5761, https://doi.org/10.1007/s00382-019-04895-x, 2019.

Wang, J., Lu, X., Yan, Y., Zhou, L., and Ma, W.: Spatiotemporal characteristics of $PM_{2.5}$ concentration in the Yangtze River Delta urban agglomeration, China on the application of big data and wavelet analysis, Sci. Total Environ., 724, 138134, https://doi.org/10.1016/j.scitotenv.2020.138134, 2020.

Wang, X.: Air Quality and Weather, https://quotsoft.net/air/, last access: 27 January 2025.

Wang, X., Zhang, R., Tan, Y., and Yu, W.: Dominant synoptic patterns associated with the decay process of $PM_{2.5}$ pollution episodes around Beijing, Atmos. Chem. Phys., 21, 2491–2508, https://doi.org/10.5194/acp-21-2491-2021, 2021.

Weare, B. C. and Nasstrom, J. S.: Examples of extended empirical orthogonal function analyses, Mon. Weather Rev., 110, 481–485, https://doi.org/10.1175/1520-0493(1982)110<0481:EOEEOF>2.0.CO;2, 1982.

Wu, B. and Wang, J.: Winter Arctic oscillation, Siberian High and EAWM, Geophys. Res. Lett., 29, 1897, https://doi.org/10.1029/2002gl015373, 2002.

Wu, D., Zhao, S., Li, J., and Wang, W.: Influences of atmospheric intraseasonal oscillation in mid–high latitudes on winter haze pollution over the Beijing-Tianjin-Hebei region, Int. J. Climatol., 43, 3173–3188, https://doi.org/10.1002/joc.8023, 2023.

Wu, G., Li, Z., Fu, C., Zhang, X., and Huang, R.: Advances in studying interactions between aerosols and monsoon in China, Sci. China. Earth. Sci., 59, 1–16, https://doi.org/10.1007/s11430-015-5198-z, 2016.

Wu, X., He, S., Guo, J., and Sun, W.: A multi-scale periodic study of $PM_{2.5}$ concentration in the Yangtze River Delta of China based on Empirical Mode Decomposition-Wavelet Analysis, China, J. Clean. Prod., 281, 124853, https://doi.org/10.1016/j.jclepro.2020.124853, 2021.

Xu, C., Ma, Y. M., Panday, A., Cong, Z. Y., Yang, K., Zhu, Z. K., Wang, J. M., Amatya, P. M., and Zhao, L.: Similarities and differences of aerosol optical properties between southern and northern sides of the Himalayas, Atmos. Chem. Phys., 14, 3133–3149, https://doi.org/10.5194/acp-14-3133-2014, 2014.

Xu, X., Zhao, T., Liu, F., Gong, S. L., Kristovich, D., Lu, C., Guo, Y., Cheng, X., Wang, Y., and Ding, G.: Climate modulation of the Tibetan Plateau on haze in China, Atmos. Chem. Phys., 16, 1365–1375, https://doi.org/10.5194/acp-16-1365-2016, 2016.

Yang, Q., Zhao, T., Bai, Y., Wei, J., Sun, X., Tian, Z., Hu, J., Ma, X., Luo, Y., Fu, W., and Yang, K.: Interannual variations in ozone pollution with a dipole structure over Eastern China associated with springtime thermal forcing over the Tibetan Plateau, Sci. Total Environ., 923, 171527, https://doi.org/10.1016/j.scitotenv.2024.171527, 2024a.

Yang, S., Liu, Y., Zhu, Z., and Qi, Y.: Infuence of the midhighlatitude Eurasian ISO on $PM_{2.5}$ concentration anomaly in North China during boreal winter, Clim. Dynam., 62, 2455–2474, https://doi.org/10.1007/s00382-023-07033-w, 2024b.

Yang, W., Li. J., Wang, Z., Wang, L., Dao, X., Zhu, L., Pan, X., Li, Y., Sun, Y., Ma, S., Wang, W., Chen, X., and Wu, J.: Source apportionment of $PM_{2.5}$ in the most polluted Central Plains Economic Region in China: Implications for joint prevention and control of atmospheric pollution, J. Clean. Prod., 283, 124557, https://doi.org/10.1016/j.jclepro.2020.124557, 2021a.

Yang, Y., Zhou, Y., Li, K., Wang, H., Ren, L., Zeng, L., Li, H., Wang, P., Li, B., and Liao, H.: Atmospheric circulation patterns conducive to severe haze in eastern China have shifted under climate change, Geophys. Res. Lett., 48, e2021GL095011, https://doi.org/10.1029/2021gl095011, 2021b.

Yu, C., Zhao, T., Bai, Y., Zhang, L., Kong, S., Yu, X., He, J., Cui, C., Yang, J., You, Y., Ma, G., Wu, M., and Chang, J.: Heavy air pollution with a unique "non-stagnant" atmospheric boundary layer in the Yangtze River middle basin aggravated by regional transport of $PM_{2.5}$ over China, Atmos. Chem. Phys., 20, 7217–7230, https://doi.org/10.5194/acp-20-7217-2020, 2020.

Zhang, Q., Zheng, Y., Tong, D., Shao, M., Wang, S., Zhang, Y., Xu, X., Wang, J., He, H., Liu, W., Ding, Y., Lei, Y., Li, J., Wang, Z., Zhang, X., Wang, Y., Cheng, J., Liu, Y., Shi, Q., Yan, L., Geng, G., Hong, C., Li, M., Liu, F., Zheng, B., Cao, J., Ding, A., Gao, J., Fu, Q., Huo, J., Liu, B., Liu, Z., Yang, F., He, K., and Hao, J.: Drivers of improved $PM_{2.5}$ air quality in China from 2013 to 2017, P. Natl. Acad. Sci. USA, 116, 24463–24469, https://doi.org/10.1073/pnas.1907956116, 2019.

Zhang, X., Xu, X., Ding, Y., Liu, Y., Zhang, H., Wang, Y., and Zhong, J.: The impact of meteorological changes from 2013 to 2017 on $PM_{2.5}$ mass reduction in key regions in China, Sci. China Earth Sci., 62, 1885–1902, https://doi.org/10.1007/s11430-019-9343-3, 2019.

Zhang, X. Y., Wang, Y. Q., Niu, T., Zhang, X. C., Gong, S. L., Zhang, Y. M., and Sun, J. Y.: Atmospheric aerosol compositions in China: spatial/temporal variability, chemical signature, regional haze distribution and comparisons with global aerosols, Atmos. Chem. Phys., 12, 779–799, https://doi.org/10.5194/acp-12-779-2012, 2012.

Zhang, Y., Ding, A., Mao, H., Nie, W., Zhou, D., Liu, L., Huang, X., and Fu, C.: Impact of synoptic weather patterns and inter-decadal climate variability on air quality in the North China Plain during 1980–2013, Atmos. Environ., 124, 119–128, https://doi.org/10.1016/j.atmosenv.2015.05.063, 2016.

Zhao, S., Feng, T., Tie, X., Dai, W., Zhou, J., Long, X., Li, G., and Cao, J.: Short-term weather patterns modulate air quality in eastern China during 2015–2016 winter, J. Geophys. Res.-Atmos., 124, 986–1002, https://doi.org/10.1029/2018jd029409, 2019.

Zheng, B., Tong, D., Li, M., Liu, F., Hong, C., Geng, G., Li, H., Li, X., Peng, L., Qi, J., Yan, L., Zhang, Y., Zhao, H., Zheng, Y., He, K., and Zhang, Q.: Trends in China's anthropogenic emissions since 2010 as the consequence of clean air actions, Atmos. Chem. Phys., 18, 14095–14111, https://doi.org/10.5194/acp-18-14095-2018, 2018a.

Zheng, Z., Ren, G., Wang, H., Dou, J., Gao, Z., Duan, C., Li, Y., Ngarukiyimana, J. P., Zhao, C., Cao, C., Jiang, M., and Yang, Y.: Relationship between fine-particle pollution and the urban heat island in Beijing, China: observational evidence, Bound.-Lay. Meteorol., 169, 93–113, https://doi.org/10.1007/s10546-018-0362-6, 2018b.

Zhong, J., Zhang, X., Dong, Y., Wang, Y., Liu, C., Wang, J., Zhang, Y., and Che, H.: Feedback effects of boundary-layer meteorological factors on cumulative explosive growth of PM2.5 during winter heavy pollution episodes in Beijing from 2013 to 2016, Atmos. Chem. Phys., 18, 247–258, https://doi.org/10.5194/acp-18-247-2018, 2018.

Zhu, W., Xu, X., Zheng, J., Yan, P., Wang, Y., and Cai, W.: The characteristics of abnormal wintertime pollution events in the Jing-Jin-Ji region and its relationships with meteorological factors, Sci. Total Environ., 626, 887–898, https://doi.org/10.1016/j.scitotenv.2018.01.083, 2018.